ADVANCED MATERIALS
www.advmat.de

Mapping Local Quantum Capacitance and Charged Impurities in Graphene via Plasmonic Impedance Imaging

Xiaonan Shan, Shan Chen, Hui Wang, Zixuan Chen, Yan Guan, Yixian Wang, Shaopeng Wang, Hong-Yuan Chen, and Nongjian Tao**

Quantum capacitance is a fundamental property of electronic materials, and relevant to many applications of the materials. This is especially the case for graphene, because unlike many other materials it has low density of states (DOS) near the Dirac point, and its capacitance is dominated by quantum capacitance.[1–5] Studying the quantum capacitance of graphene is thus important for understanding 2D materials, and for developing electronic and energy storage applications, such as supercapacitors.[6–20] The total energy storage capacity is determined by the specific surface area and quantum capacitance of graphene.[13,16,20–22] The former is extremely large for atomically thin graphene, but the latter is nearly zero at the Dirac point according to the theory for ideal graphene.[1,3,23] The quantum capacitance of real graphene samples has been measured, but the measured quantum capacitance is averaged over the entire sample.[1–3] Due to the heterogeneous nature of graphene samples,[24–28] a capability to map the local quantum capacitance is thus necessary. Scanning gate microscopy[2,29,30] and scanning single-electron transistor microscopy[31,32] are powerful tools for probing surface conductance and charge of graphene, however, the use of a scanning probe and complexity of the instrumentation limit their applications, especially in aqueous solutions and electrolytes.

We developed a plasmonics-based electrical impedance microscopy (P-EIM) method to map the local quantum capacitance of graphene supported on a substrate. By mapping the local quantum capacitance as a function of potential, we determined both the local density and polarity of charged impurities, and mapped the electron and hole puddles associated with charged impurities in graphene. We further showed that the local quantum capacitance and charge density could be controlled by modifying the supporting substrate with molecules terminated with different charged groups. We anticipate that the P-EIM method can be applied to study the surface capacitance and charge distribution of other nano and 2D materials.

Dr. X. Shan, S. Chen, Z. Chen, Dr. Y. Guan, Dr. Y. Wang, Dr. S. Wang, Prof. N. Tao
Center for Bioelectronics and Biosensors
Biodesign Institute
Arizona State University
Tempe, AZ 85287, USA
E-mail: Nongjian.Tao@asu.edu
H. Wang, Prof. H.-Y. Chen, Prof. N. Tao
State Key Laboratory of Analytical Chemistry for Life Science
School of Chemistry and Chemical Engineering
Nanjing University
Nanjing 210093, China
E-mail: hychen@nju.edu.cn

DOI: 10.1002/adma.201502822

Traditionally, capacitance is measured by detecting a current or charge response of a system to a voltage change, which is widely used, but does not provide imaging capability. By contrast, P-EIM measures the local impedance optically, allowing for imaging of local interfacial capacitance. This new approach also minimizes parasitic capacitance, a common complication in electrical measurement.[33–36] The basic principle of P-EIM is the sensitive dependence of surface plasmon frequency on surface charge density, $\Delta\sigma$, which is related to local interfacial capacitance per unit area, c, $\Delta\sigma = c \cdot \Delta V$, where ΔV is the applied potential.[33,37]

Figure 1a illustrates the principle and experimental setup, showing a graphene sample placed on a gold film on top of the objective of an inverted optical microscope. The sample surface was immersed in 0.2 M NaF, and the potential of the gold film was controlled with respect to a Ag/AgCl reference electrode in the electrolyte.[38,39] Light from a superluminescent diode (SLED) was directed onto the gold film to excite surface plasmons at the surface of the gold film, and the reflected light was directed to a charge coupled device (CCD) imager via the same objective to form a plasmonic image of the graphene. Surface plasmons are excited on gold film by light with incident angle tuned to an appropriate angle (resonant angle), and this angle is extremely sensitive to the refractive index change near the gold film. The addition of a graphene layer onto the gold surface will change the refractive index, and thus the resonant angle, which is imaged by the CCD imager. In order to measure the quantum capacitance of graphene, a periodic modulation with angular frequency of ω was superimposed on the potential applied to the gold film, which created a periodic modulation in surface charge density, $\Delta\sigma$. We have shown previously that associated with the surface charge modulation is a plasmonic image intensity modulation (expressed in terms of resonance angle shift), $\Delta\theta(x,y,\omega)$, given by $\Delta\sigma(x,y,\omega) = \alpha\Delta\theta(x,y,\omega)$, where α is 47 C m^{-2} deg^{-1}.[33] The plasmonic image intensity modulation was determined by performing Fourier transform of each pixel recorded with the CCD, allowing us to obtain a capacitance image according to $c(x,y,z) = \Delta\sigma/\Delta V = \alpha\Delta\theta(x,y,z)/\Delta V$. Note that the traditional plasmonic images of the sample can be simultaneously obtained with the same setup by removing the periodic modulation component in the plasmonic image intensity. The setup also allows us to obtain the bright-field image of graphene.

Using P-EIM, we imaged the interfacial capacitance of single- and double-layer graphene. Both the plasmonic and bright-field images provided information on the thickness of the graphene sample (see the Supporting Information). Figure 1b shows the plasmonic (left) and bright-field (right) images of a single layer graphene. Raman spectrum of the sample further confirmed

ADVANCED MATERIALS
www.advmat.de

www.MaterialsViews.com

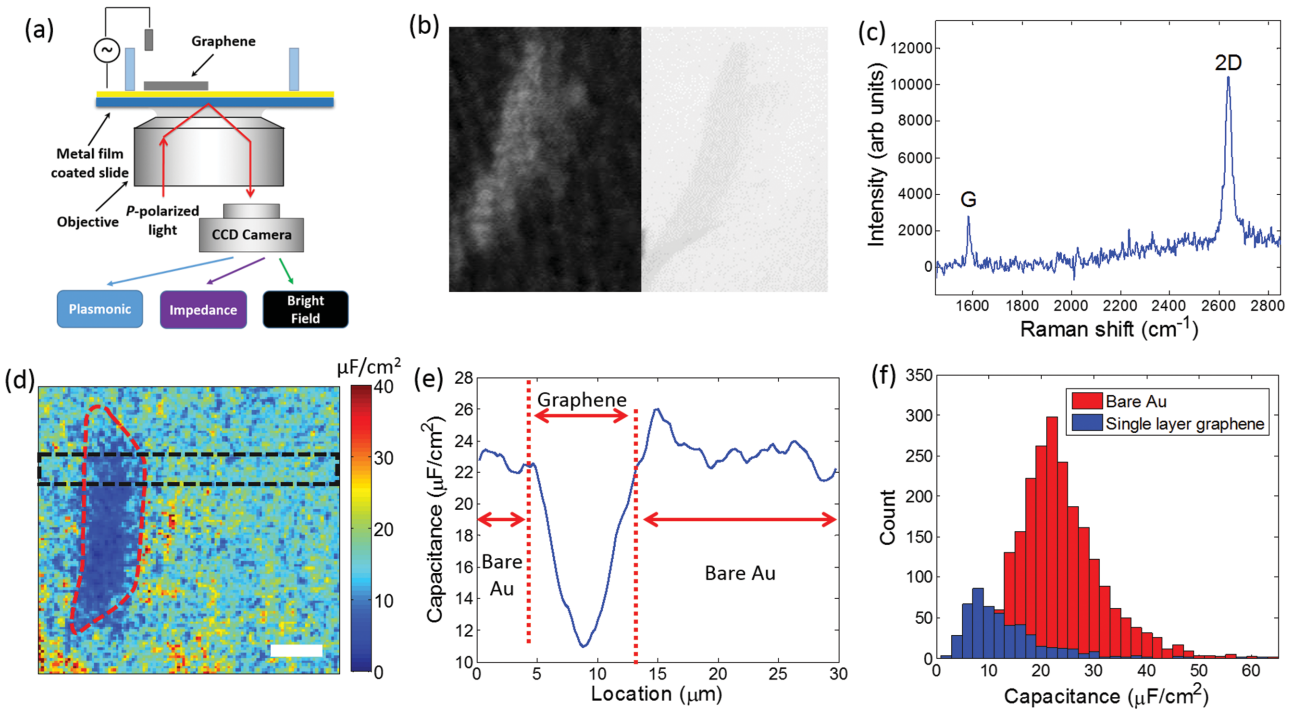

Figure 1. Imaging of local quantum capacitance of graphene with P-EIM. a) Experiment setup for simultaneous plasmonic, impedance (quantum capacitance), and bright field images of graphene. b) Plasmonic image (left) and bright field image (right) of a single layer graphene. c) Raman spectrum of the single layer graphene sample. d) Quantum capacitance of single layer graphene (outlined with red dashed line). Scale bar: 5 μm. e) Local distribution of capacitance across the single layer graphene along the box region shown in (d). f) Capacitance distributions of the single layer graphene and the surrounding bare Au area.

that the sample was single layer graphene (Figure 1c). Figure 1d shows the local interfacial capacitance of a single layer graphene sample at the Dirac point (–0.08 V vs Ag/AgCl). The average interfacial capacitance of the graphene at the Dirac point is about 7 μF cm^{-2}, much smaller than the interfacial capacitance of gold, which is ≈25 μF cm^{-2}, but significantly larger than the predicted value (≈0.8 μF cm^{-2}) for ideal graphene. The interfacial capacitance is not uniform across the graphene sample, and the values near the edge of the graphene are higher than the central region of the graphene. This is clearly shown in the capacitance cross-section plot (Figure 1e). Figure 1f is the histogram of the local capacitance of the graphene, which reveals a broad distribution with a peak at ≈7 μF cm^{-2}. This nonzero value and broad distribution of capacitance of graphene at the Dirac point are due to local charged impurities. We will return to this later.

The interfacial capacitance measured by P-EIM in graphene area consists of two major contributions: electrical double layer capacitance (C_{EDL}) and quantum capacitance (C_G) as shown in **Figure 2**a. Note that the diffuse layer capacitance is relative small compared with quantum capacitance and electrical double layer capacitance. These two contributions are modeled as two capacitors in series, and the quantum capacitance of graphene is given by $\frac{1}{C_G} = \frac{1}{C} - \frac{1}{C_{EDL}}$, where C is the measured interfacial capacitance. C_{EDL} can be obtained from the interfacial capacitance in the area of bare gold surface, where only the electrical double layer capacitance contributes to the measured interfacial capacitance. In 0.2 M NaF, C_{EDL} is about 25 μF cm^{-2}. Using this value, we obtained the graphene quantum capacitance from the interfacial capacitance imaged with P-EIM. Figure 2d–f shows the local quantum capacitance of the single layer graphene at different offset potentials (the entire area is covered with graphene). The graphene was transferred onto the Au film with poly (methyl-methacrylate) (PMMA)-mediated method (see the Supporting Information). The average quantum capacitance is 3–5 μF cm^{-2} for single layer graphene at the Dirac point (Figure 2e). Note that the two-capacitor model contains only one unknown parameter, the quantum capacitance. Because the quantum capacitance is small compared to the double layer capacitance, it dominates the total interfacial capacitance of graphene. In other words, an error in the double layer capacitance results in a smaller error in the quantum capacitance. Furthermore, the model was supported by the previous electrical measurement of quantum capacitance.[3]

The quantum capacitance of graphene is related to the density of states of graphene, which can be tuned by shifting the Fermi energy level of the electrode (gold film) with an applied potential. At the Dirac point, the density of states of an ideal single layer graphene is zero. Moving the Fermi level either above or below the Dirac point, the density of states increases proportionally, corresponding to the occupation of either n- (electrons) or p-type (holes) carriers. Consequently, the quantum capacitance displays a V-shape dependence on the Fermi energy level given by[40]

$$C_Q \approx e^2 \frac{2}{\pi} \frac{eV_{ch}}{(\hbar v_F)^2} \quad (1)$$

DOI: 10.1002/adma.201502822

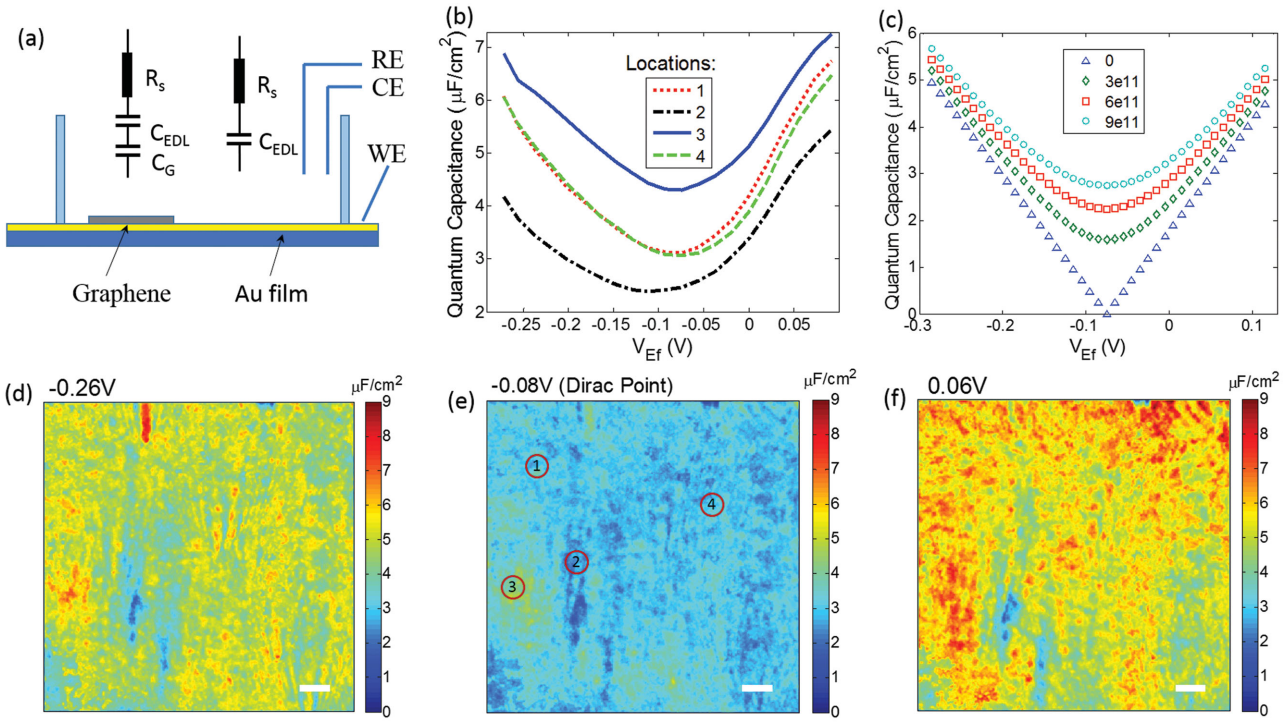

Figure 2. Quantum capacitance versus potential. a) Schematic illustration of quantum capacitance measurement, where WE, RE, and CE denote working, reference, and counter electrodes, respectively, for a standard three-electrode electrochemical setup. The equivalent circuits of the graphene area (left) and bare Au region (right) are shown with R_s, C_{EDL}, and C_G representing the solution resistance, double layer capacitance, and graphene capacitance, respectively. b) Measured graphene quantum capacitance versus potential at different locations marked in (e). c) Theoretical graphene quantum capacitance versus potential at different impurities. d–f) Local quantum capacitance of graphene at different potentials: d) −0.26 V, e) −0.08 V (Dirac point), and f) 0.06 V. Scale bar: 5 μm.

where $\hbar$ is the Planck constant, e is the electron charge, v_F is the Fermi velocity of Dirac electrons, $\approx c/300$ (c is the speed of light in a vacuum), and V_{ch} is the graphene potential, respectively. We imaged the local quantum capacitance at different potentials by sweeping the electrode potential (Movie S1, Supporting Information). Figure 2d–f are few snapshots at, above, and below the Dirac point, respectively. The average quantum capacitance values above and below the Dirac point are higher than the value at the Dirac point, which is expected according to Equation (1). The quantum capacitance images at different potentials also reveal large local variations, which are not described by Equation (1).

Figure 2b plots the local quantum capacitance versus potential at different locations, which shows substantial deviations from the prediction for ideal graphene. First, the measured quantum capacitance at the Dirac point is not zero, and varies from location to location. Second, the potential of the Dirac point (the potential of the minimum capacitance) also varies from location to location. It has been reported that the charged impurities lead to local potential fluctuations, which give rise to an additional electron or hole density n^* near the impurity sites.[41] These electron- and hole-rich regions have been referred to as electron and hole puddles.[32,41] The charge impurities and associated electron and hole puddles affect graphene transport properties, but also quantum capacitance. By including the additional carrier density associated with the charge impurities or defects, quantum capacitance can be expressed by[3]

$$C_Q = \frac{2e^2}{\hbar v_F \sqrt{\pi}} \left(|n_G| + |n^*| \right)^{1/2} \quad (2)$$

where $n_G = \left(\frac{e(V_{ch} - V_o)}{\hbar v_F \sqrt{\pi}} \right)^2$ and n^* are the carrier concentrations caused by the applied potential and charged impurities, respectively. Note that V_o is an offset potential of the Dirac point, which varies with the local charge impurities. Figure 2c plots the quantum capacitance of graphene versus potential at different impurity densities determined by Equation (2), where V_{ch} is related to the applied potential V_b, by $V_{ch} = V_b C_{EDL} / (C_{EDL} + C_Q)$. A comparison of panels (b) and (c) of Figure 2 indicates that the experiment results can be explained well by including the impurity-induced carrier concentration (n^*) in the model. The best fit of the measured average quantum capacitance with Equation (2) leads to $n^* = 9 \times 10^{11}$ cm^{-2}, which is consistent with the literature data.[41,42] We note that the experimental quantum capacitance versus potential shows an asymmetry with respect to the Dirac point, which may be attributed to asymmetric impurity density distribution (Supporting Information).[32,43,44]

The charged impurity model provides a quantitative explanation of the experimental data. One possible source of charged impurities is from the supporting substrate (gold film).[41] In order to further understand the effect of the substrate charged impurities on graphene quantum capacitance, we modified the gold substrate with thiol molecules, cysteamine, and

3-mercaptopropionic acid (**Figure 3**a). Both molecules can bind to the gold substrate, but the former is terminated with a positive charge, and the latter with a negative charge. Graphene was placed on top of the cysteamine and 3-mercaptopropionic acid-modified gold substrates. Note that the surface coverages of the thiol molecules were controlled to ensure good electrical contact between the graphene sample and the gold substrate (see the Experimental Section).

With positive charges on the substrate surface, the Fermi level is expected to shift above the Dirac point (Figure 3a). On the other hand, coating the substrate surface with negative charges, the Fermi level is expected to shift below the Dirac point (Figure 3a). Indeed, we found that the quantum capacitance minimum shifted toward negative potentials for cysteamine-modified gold substrate (positive charges), and positive potentials for 3-mercaptopropionic acid-modified gold substrate (negative charge) (Figure 3b). For comparison, the quantum capacitance versus potential plot for graphene on an unmodified gold substrate is also shown (blue curve). In addition to shifting the potential of minimum quantum capacitance, the charged impurities also increase the value of the minimum quantum capacitance, which can be attributed to the extra impurity density, according to Equation (2).

The plots in Figure 3b are quantum capacitance averaged over the entire graphene sample, where the potential of minimum quantum capacitance reflects the polarity and magnitude of charged impurities. Because charged impurities are in general not uniformly distributed over the entire surface, it is important to obtain the local potential of minimum quantum capacitance or offset voltage (V_o). We obtained V_o at each location (pixel) by plotting the quantum capacitance versus applied potential, which are shown in Figure 3c,e,g. These potentials of minimum quantum capacitance images reveal heterogeneous distributions of charged impurities on the charge-modified and unmodified substrates. The degree of the heterogeneity in each case is more clearly shown in the histograms of the potentials of minimum quantum capacitance plotted in Figure 3d,f,h. These results show that the modification of the substrate with charged molecules can change the charge carries in the graphene,[45,46] and the spatial distribution of the interfacial molecules can be imaged with the present P-EIM.

Charged impurities have a profound impact on quantum capacitance as shown here, and also on the charge transport properties, such as mobility, of graphene field effect devices.[41,42] They affect the charge transport and quantum capacitance of graphene by forming local electron or hole puddles, and mapping the charge density and polarity of these puddles are thus important. We obtained both the charge density and polarity from the potential and value of the minimum quantum capacitance at each pixel of the P-EIM images. **Figure 4**a plots the impurity density image obtained with Equation (2), showing that the local impurity density can vary from 1×10^{12} per cm^2 to 3.3×10^{12} per cm^2. Figure S4 (Supporting Information) plots the histogram of the local potential of minimum quantum capacitance, showing a distribution in both positive and negative charges with respect to the Dirac point. The spatial distribution of the positive and negative charged impurities or electron and hole puddles is shown in Figure 4b. It reveals several interesting features: (1) At the Dirac point, both the electron and hole puddles coexist, (2) the sizes of the electron and hole puddles vary over wide range, and (3) the electron and hole puddles are not uniformly mixed and within certain regions are either prominently electron or hole puddles.

Density of states (DOS) describes the number of states per interval of energy at each energy level and it determines the quantum capacitance of graphene. When $E_F \gg k_B T$,

$$C_Q = e^2 \frac{dn}{d\mu} = Se^2 D_{tot}, \quad (3)$$

where n is carrier concentration, μ is chemical potential, S is area of the graphene, and D_{tot} is total DOS of graphene including DOS from the impurities. The impurity contribution to the measured DOS is[4,43]

$$D_{it}(x,y,E_f) = \frac{1}{e^2}\left(C_Q(x,y,E_f) - C_{QM}(x,y,E_f)\right) \quad (4)$$

where C_Q is the measured quantum capacitance and C_{QM} is the quantum capacitance for ideal graphene (Equation S1, Supporting Information). From Equation (4), we obtained the local impurity density of states, D_{it}, shown in Figure 4c, which reveals a broad peak near the Fermi level. The impurity density of states is not uniform across the entire sample, which is shown in Figure 4d.

Graphene is a 2D material with interesting potential applications because of its unique properties, including its electrical capacitance. Unlike most other conducting materials, graphene's density of states at the Dirac point is zero. Consequently, its capacitance is dominated by quantum effect, instead of classical electrostatic origin. Determining and understanding graphene's quantum capacitance properties are thus critical for developing field effect electronic devices and energy-storage materials with graphene. Traditionally, capacitance is usually measured electrically, which can only provide an average capacitance over the entire sample. In this work, we developed a plasmonic imaging approach, which converts the electrical signal into a plasmonic signal, and then imaged optically. This approach allowed us to image the local quantum capacitance, as well as charge impurity density and impurity density of states.

Our studies revealed several new aspects of graphene and its quantum capacitance. First, the graphene's capacitance is small compared with the gold electrode, but it is much larger than the theoretical prediction of ideal quantum capacitance, which is attributed to charge impurities. We confirm the charge impurity effect by modifying the substrate surface with defined charges. Second, the quantum capacitance varies from location to location, reflecting local variation in the charge impurity density. For example, the edge areas of graphene tend to have larger quantum capacitance than the center areas. Third, the potential of the Dirac point is different from location to location, which is caused by the local variations in both the polarity and magnitude of the charge impurity. Finally, our study suggests that graphene with charged impurities may help increase graphene capacitance, and thus the energy storage capacity of the material.

In summary, we have demonstrated a plasmonic imaging method to map local quantum capacitance of graphene. The

Adv. Mater. **2015**,
DOI: 10.1002/adma.201502822

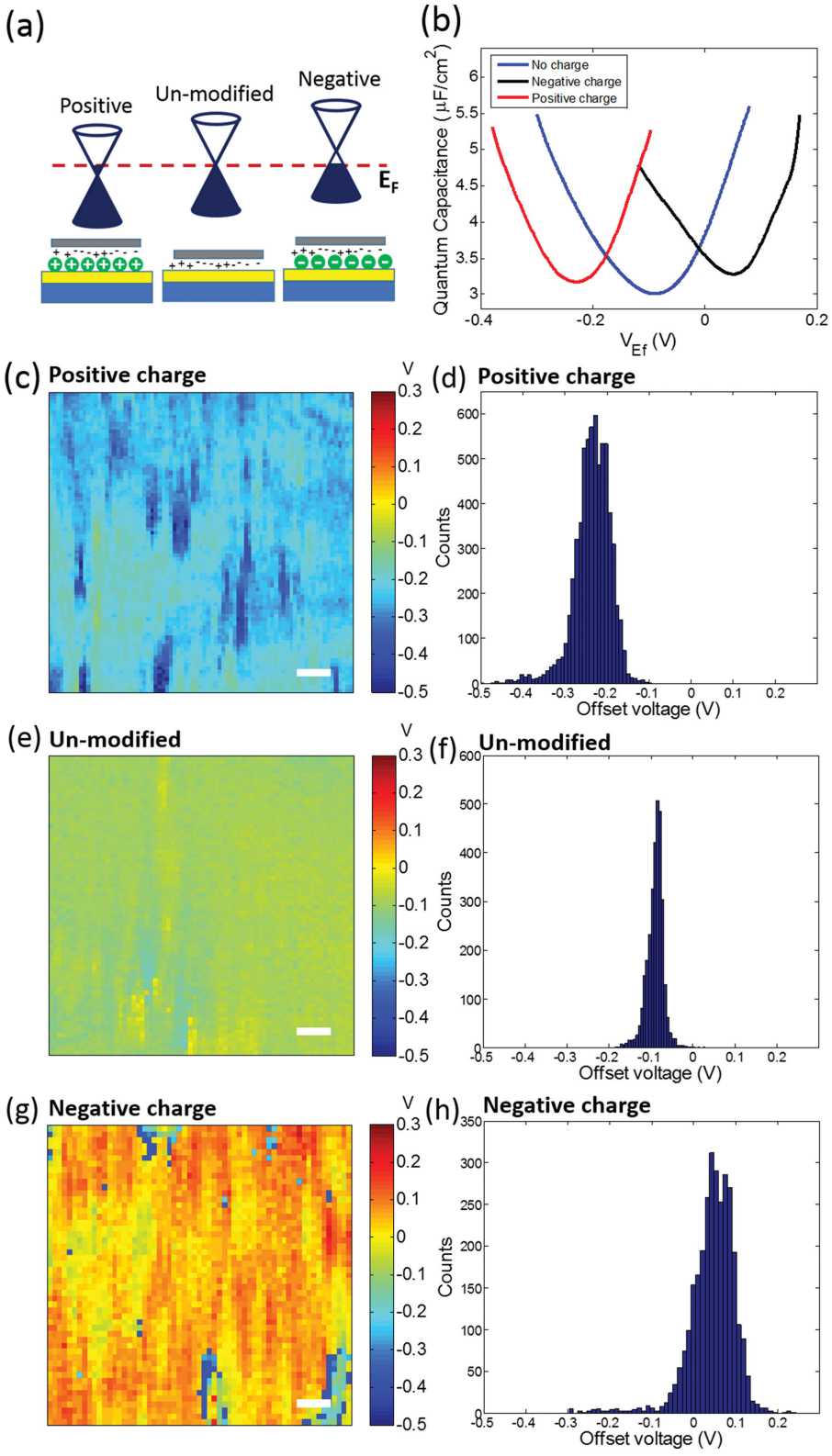

Figure 3. Effect of interfacial charges on graphene quantum capacitance. a) Energy diagrams of graphene under different interfacial charge conditions (upper panel). Introduction of interfacial charges on the substrate with thiol molecules with positively and negatively charged terminals (lower panel). b) Quantum capacitance versus potential plots for different interfacial conditions: unmodified (blue), positive (red), and negative (black) charge. c,e,g) Mapping local Dirac point shift of graphene under influence of different interfacial conditions. d,f,h) Histograms of Dirac point shift under different interfacial conditions.

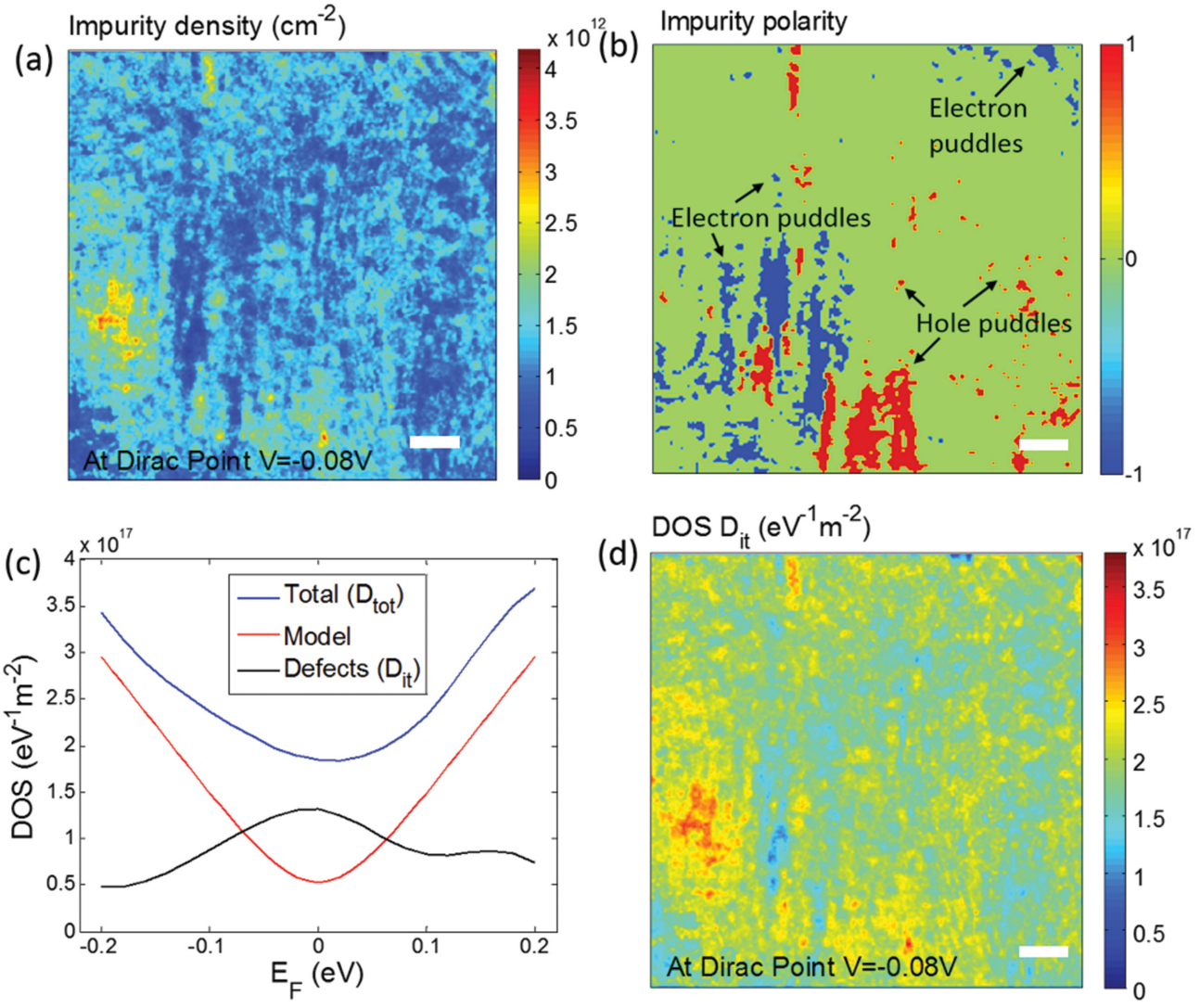

Figure 4. Local impurity density, electron and hole puddles, and density of states. a) Local charge impurity density of graphene at Dirac point (V = –0.08 V). b) Electron (blue) and hole (red) puddles at the average Dirac point. c) Total measured (blue), ideal (red), and extracted impurity densities of states of graphene. Blue curve is the total DOS (D_{tot}) including the DOS from ideal graphene and defects. Red curve is the model DOS calculated from Equation (3). Black curve is the DOS of defects and impurities. d) Local impurity density of state at the Dirac point.

method converts an electrical signal into a surface plasmon response, which is imaged optically. We have shown that the measured quantum capacitance deviates significantly from the theoretical prediction for an ideal graphene, and explained the data quantitatively in terms of charged impurities. We further confirm the role of charged impurities by controlling the substrate surface charge with molecules terminated with different charged groups. Finally, from the local quantum capacitance and its dependence on applied potential, we have obtained the magnitude of surface density and polarities of charged impurities, and obtained images of the electron and hole puddles in graphene. The study reveals important roles of charged impurities on the quantum capacitance of graphene, which is relevant to electronic and energy storage applications of the material. We anticipate that the method can be applied to map local capacitance and charge impurities of other nano and 2D materials.

Experimental Section

Graphene Transfer and Electrochemical Setup: Graphene was transferred by both mechanical exfoliation of Kish graphite and poly (methylmethacrylate) (PMMA) mediated approach. Mechanical exfoliation of Kish graphite is using to obtain graphene sample in the Figure 1. The electronics grade dicing tape is used to minimize contaminations, and the graphene was then transferred onto the gold thin film (prepared by coating a glass slide with 2 nm chromium adhesion layer followed with 47 nm gold). To minimize contaminants on the gold film, it was cleaned with hydrogen flame before the transfer of graphene. After graphene transfer, the surface was rinsed with ethanol and then dried with nitrogen gas. PMMA mediated approach was used for Figures 2– 4, where the entire surface was covered with graphene grown by chemical vapor deposition (purchased from Graphene Supermarket). The same cleaning process was used to minimize the contamination.

An electrochemical cell made of Teflon was placed on top of the gold film, and 0.2 M NaF solution was used as electrolyte. We controlled the graphene potential with respect to Ag/AgCl reference electrode with a

Adv. Mater. **2015**,
DOI: 10.1002/adma.201502822

potentiostat (Pine Research Instrumentation) using a platinum coil as counter electrode. Superimposed on the potential was a sinusoidal potential with frequency of 80 Hz and amplitude of 0.05 V (see more details in the Supporting Information).

Optical Setup and Imaging Processing: For plasmonic imaging, p-polarized light with wavelength 680 nm from a SLED (QPhotonics) was directed on the gold film via the objective of an inverted optical microscope, and the plasmonic image was formed with the same objective and recorded with a CCD camera (AVT Pike F-032B). The potential dependent component of the plasmonic image intensity at each pixel was processed to produce an interfacial capacitance image of the surface.

Surface Charge Modification: 1×10^{-3} M cysteamine and 3-mercaptopropionic acid solutions were used to modify the gold substrate with positive and negative charges, respectively. Before the modification, the Au film was cleaned with hydrogen flame. The hydrogen flame-cleaned Au film was immersed into one of the solution for 10 s, and then rinsed with deionized water thoroughly. The Au film was dried with nitrogen and the graphene was transferred onto the Au film.

Supporting Information

Supporting Information is available from the Wiley Online Library or from the author.

Acknowledgements

The support of this work by the AFOSR MURI (Grant FA9550-14-0003), Keck Foundation, and Gordon and Betty Moore Foundation is gratefully acknowledged.

Received: June 11, 2015
Revised: July 16, 2015
Published online:

[1] H. L. Xu, Z. Y. Zhang, Z. X. Wang, S. Wang, X. L. Hang, L. M. Peng, *ACS Nano* **2011**, *5*, 2340.
[2] F. Giannazzo, S. Sonde, V. Raineri, E. Rimini, *Nano Lett.* **2009**, *9*, 23.
[3] J. L. Xia, F. Chen, J. H. Li, N. J. Tao, *Nat. Nanotechnol.* **2009**, *4*, 505.
[4] G. L. Yu, R. Jalil, B. Belle, A. S. Mayorov, P. Blake, F. Schedin, S. V. Morozov, L. A. Ponomarenko, F. Chiappini, S. Wiedmann, U. Zeitler, M. I. Katsnelson, A. K. Geim, K. S. Novoselov, D. C. Elias, *Proc. Natl. Acad. Sci. USA* **2013**, *110*, 3282.
[5] S. Ilani, L. A. K. Donev, M. Kindermann, P. L. McEuen, *Nat. Phys.* **2006**, *2*, 687.
[6] F. Bonaccorso, L. Colombo, G. Yu, M. Stoller, V. Tozzini, A. C. Ferrari, R. S. Ruoff, V. Pellegrini, *Science* **2015**, *347*, 41.
[7] M. A. Green, K. Emery, Y. Hishikawa, W. Warta, E. D. Dunlop, *Prog. Photovolt.* **2013**, *21*, 827.
[8] Y. Gogotsi, P. Simon, *Science* **2011**, *334*, 917.
[9] X. Yang, C. Cheng, Y. Wang, L. Qiu, D. Li, *Science* **2013**, *341*, 534.
[10] M. Z. Liu, M. B. Johnston, H. J. Snaith, *Nature* **2013**, *501*, 395.
[11] X. Wang, L. J. Zhi, K. Mullen, *Nano Lett.* **2008**, *8*, 323.
[12] N. L. Yang, J. Zhai, D. Wang, Y. S. Chen, L. Jiang, *ACS Nano* **2010**, *4*, 887.
[13] Y. W. Zhu, S. Murali, M. D. Stoller, K. J. Ganesh, W. W. Cai, P. J. Ferreira, A. Pirkle, R. M. Wallace, K. A. Cychosz, M. Thommes, D. Su, E. A. Stach, R. S. Ruoff, *Science* **2011**, *332*, 1537.
[14] J. R. Miller, R. A. Outlaw, B. C. Holloway, *Science* **2010**, *329*, 1637.
[15] Z. S. Wu, W. C. Ren, D. W. Wang, F. Li, B. L. Liu, H. M. Cheng, *ACS Nano* **2010**, *4*, 5835.
[16] K. S. Novoselov, V. I. Fal'ko, L. Colombo, P. R. Gellert, M. G. Schwab, K. Kim, *Nature* **2012**, *490*, 192.
[17] M. D. Stoller, S. J. Park, Y. W. Zhu, J. H. An, R. S. Ruoff, *Nano Lett.* **2008**, *8*, 3498.
[18] P. Simon, Y. Gogotsi, *Nat. Mater.* **2008**, *7*, 845.
[19] D. S. Yu, K. Goh, H. Wang, L. Wei, W. C. Jiang, Q. Zhang, L. M. Dai, Y. Chen, *Nat. Nanotechnol.* **2014**, *9*, 555.
[20] M. F. El-Kady, V. Strong, S. Dubin, R. B. Kaner, *Science* **2012**, *335*, 1326.
[21] Q. Wu, Y. X. Xu, Z. Y. Yao, A. R. Liu, G. Q. Shi, *ACS Nano* **2010**, *4*, 1963.
[22] Y. Zhu, S. Murali, M. D. Stoller, A. Velamakanni, R. D. Piner, R. S. Ruoff, *Carbon* **2010**, *48*, 2118.
[23] Y. Li, Z. Li, P. K. Shen, *Adv. Mater.* **2013**, *25*, 2474.
[24] L. Britnell, R. M. Ribeiro, A. Eckmann, R. Jalil, B. D. Belle, A. Mishchenko, Y. J. Kim, R. V. Gorbachev, T. Georgiou, S. V. Morozov, A. N. Grigorenko, A. K. Geim, C. Casiraghi, A. H. Castro Neto, K. S. Novoselov, *Science* **2013**, *340*, 1311.
[25] Y. Hao, M. S. Bharathi, L. Wang, Y. Liu, H. Chen, S. Nie, X. Wang, H. Chou, C. Tan, B. Fallahazad, H. Ramanarayan, C. W. Magnuson, E. Tutuc, B. I. Yakobson, K. F. McCarty, Y.-W. Zhang, P. Kim, J. Hone, L. Colombo, R. S. Ruoff, *Science* **2013**, *342*, 720.
[26] J. M. Cai, P. Ruffieux, R. Jaafar, M. Bieri, T. Braun, S. Blankenburg, M. Muoth, A. P. Seitsonen, M. Saleh, X. L. Feng, K. Mullen, R. Fasel, *Nature* **2010**, *466*, 470.
[27] Q. J. Xiang, J. G. Yu, M. Jaroniec, *J. Am. Chem. Soc.* **2012**, *134*, 6575.
[28] J. Haskins, A. Kinaci, C. Sevik, H. Sevincli, G. Cuniberti, T. Cagin, *ACS Nano* **2011**, *5*, 3779.
[29] R. Jalilian, L. A. Jauregui, G. Lopez, J. Tian, C. Roecker, M. M. Yazdanpanah, R. W. Cohn, I. Jovanovic, Y. P. Chen, *Nanotechnology* **2011**, *22*, 295705.
[30] N. Pascher, D. Bischoff, T. Ihn, K. Ensslin, *Appl. Phys. Lett.* **2012**, *101*, 63101.
[31] M. J. Yoo, T. A. Fulton, H. F. Hess, R. L. Willett, L. N. Dunkleberger, R. J. Chichester, L. N. Pfeiffer, K. W. West, *Science* **1997**, *276*, 579.
[32] J. Martin, N. Akerman, G. Ulbricht, T. Lohmann, J. H. Smet, K. Von Klitzing, A. Yacoby, *Nat. Phys.* **2008**, *4*, 144.
[33] K. J. Foley, X. Shan, N. J. Tao, *Anal. Chem.* **2008**, *80*, 5146.
[34] X. N. Shan, U. Patel, S. P. Wang, R. Iglesias, N. J. Tao, *Science* **2010**, *327*, 1363.
[35] X. Shan, I. Diez-Perez, L. Wang, P. Wiktor, Y. Gu, L. Zhang, W. Wang, J. Lu, S. Wang, Q. Gong, J. Li, N. Tao, *Nat. Nanotechnol.* **2012**, *7*, 668.
[36] W. Wang, K. Foley, X. Shan, S. P. Wang, S. Eaton, V. J. Nagaraj, P. Wiktor, U. Patel, N. J. Tao, *Nat. Chem.* **2011**, *3*, 249.
[37] S. P. Wang, X. P. Huang, X. N. Shan, K. J. Foley, N. J. Tao, *Anal. Chem.* **2010**, *82*, 935.
[38] X. N. Shan, S. P. Wang, W. Wang, N. J. Tao, *Anal. Chem.* **2011**, *83*, 7394.
[39] X. N. Shan, Y. M. Fang, S. P. Wang, Y. Guan, H. Y. Chen, N. J. Tao, *Nano Lett.* **2014**, *14*, 4151.
[40] D. L. John, L. C. Castro, D. L. Pulfrey, *J. Appl. Phys.* **2004**, *96*, 5180.
[41] S. Adam, E. H. Hwang, V. M. Galitski, S. D. Sarma, *Proc. Natl. Acad. Sci. USA* **2007**, *104*, 18392.
[42] S. Cho, M. S. Fuhrer, *Phys. Rev. B* **2008**, *77*, 4.
[43] L. A. Ponomarenko, R. Yang, R. V. Gorbachev, P. Blake, A. S. Mayorov, K. S. Novoselov, M. I. Katsnelson, A. K. Geim, *Phys. Rev. Lett.* **2010**, *105*, 4.
[44] S. Droscher, P. Roulleau, F. Molitor, P. Studerus, C. Stampfer, K. Ensslin, T. Ihn, *Appl. Phys. Lett.* **2010**, *96*, 3.
[45] H. T. Liu, Y. Q. Liu, D. B. Zhu, *J. Mater. Chem.* **2011**, *21*, 3335.
[46] F. Schedin, A. K. Geim, S. V. Morozov, E. W. Hill, P. Blake, M. I. Katsnelson, K. S. Novoselov, *Nat. Mater.* **2007**, *6*, 652.